Journal of Power Sources 195 (2010) 1786–1792

Contents lists available at ScienceDirect

Journal of Power Sources

journal homepage: www.elsevier.com/locate/jpowsour

Nanotubes of rare earth cobalt oxides for cathodes of intermediate-temperature solid oxide fuel cells

Joaquín Sacanell[a,b,*], A. Gabriela Leyva[a,c], Martín G. Bellino[b], Diego G. Lamas[b]

[a] Departamento de Física, Centro Atómico Constituyentes, CNEA, Av. Gral. Paz 1499, 1650 San Martín, Buenos Aires, Argentina
[b] CINSO (Centro de Investigaciones en Sólidos), CITEFA-CONICET, J.B. de La Salle 4397, 1603 Villa Martelli, Buenos Aires, Argentina
[c] Escuela de Ciencia y Tecnología, UNSAM. Av. Gral. Paz 1499, 1650 San Martín, Buenos Aires, Argentina

ARTICLE INFO

Article history:
Received 5 September 2009
Received in revised form 15 October 2009
Accepted 16 October 2009
Available online 24 October 2009

Keywords:
Nanotubes
SOFC cathodes
Cobaltites

ABSTRACT

In this work we studied the electrochemical properties of cathodes for intermediate-temperature solid oxide fuel cells (IT-SOFCs) prepared with nanotubes of $La_{0.6}Sr_{0.4}CoO_3$ (LSCO). Their nanostructures consist of agglomerated nanoparticles in tubular structures of sub-micrometric diameter. The resulting cathodes are highly porous both at the micro- and the nanoscale. This fact increases significantly the access to active sites for the oxygen reduction.

We investigated the influence of the diameter of the precursor nanotubes on the polarization resistance of the LSCO cathodes on CeO_2–10 mol.% Sm_2O_3 (SDC) electrolytes under air atmosphere, evaluated in symmetrical [LSCO/SDC/LSCO] cells. Our results indicate an optimized performance when the diameter of precursor nanotubes is sufficiently small to become dense nanorods after cathode sintering.

We present a phenomenological model that successfully explains the behavior observed and considers that a small starting diameter acts as a barrier that prevents grains growth. This is directly related with the lack of contact points between nanotubes in the precursor, which are the only path for the growth of ceramic grains.

We also observed that a conventional sintering process (of 1 h at 1000 °C with heating and cooling rates of 10 °C min^{-1}) has to be preferred against a fast firing one (1 or 2 min at 1100 °C with heating and cooling rates of 100 °C min^{-1}) in order to reach a higher performance. However, a good adhesion of the cathode can be achieved with both methods.

Our results suggest that oxygen vacancy diffusion is enhanced while decreasing LSCO particle size. This indicates that the high performance of our nanostructured cathodes is not only related with the increase of the number of active sites for oxygen reduction but also to the fact that the nanotubes are formed by nanoparticles.

1. Introduction

Fuel cells are one of the most promising devices for environmentally clean energy production by directly converting chemical energy into electricity [1,2]. Among them, solid oxide fuel cells (SOFCs) [3], have the unique capability to use different fuels such as hydrocarbons or hydrogen. However, several issues have to be solved in order to improve their efficiency and in terms of costs of operation. The reduction of the typically high working temperature which is around 900–1000 °C is one of the most important ones. For this reason, extensive research has been devoted in the last years to the study of novel materials and structures to produce cells capable to work at intermediate-temperature solid oxide fuel cells (IT-SOFCs).

In the case of the cathode, one step in this direction is the use of materials with high mixed ionic and electronic conductivity in the range of 500–800 °C [1,4]. One of the earliest studied materials meeting this requirement, was the rare earth cobalt oxide $La_{0.6}Sr_{0.4}CoO_3$ (LSCO) [5,6]. Although this compound was found to be one of the best when regarding its electrochemical properties, it has a significantly high thermal expansion coefficient compared to that of typical electrolytes. This fact makes the electrolyte–cathode attaching procedure very difficult, a problem that has been solved by doping with Fe. As a counterpart, a significant drop on the conductivity has been observed [3,7]. However, iron substituted cobaltites of the formula $Ln_{1-x}R_xCo_{1-y}Fe_yO_3$ (Ln: lanthanide, R: alkaline earth) have shown to be adequate as cathodes for IT-SOFCs [8–10].

* Corresponding author at: Departamento de Física, Centro Atómico Constituyentes, CNEA, Av. Gral. Paz 1499, 1650 San Martín, Pcia. de Buenos Aires, Argentina. Tel.: +54 11 6772 7657; fax: +54 11 6772 7121.
E-mail address: sacanell@cnea.gov.ar (J. Sacanell).

0378-7753/$ – see front matter © 2009 Elsevier B.V. All rights reserved.
doi:10.1016/j.jpowsour.2009.10.049

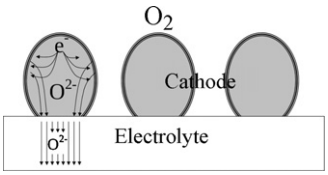

Fig. 1. Schematic representation of the active zone for oxygen reduction and transport in a porous mixed electronic/ionic conductor cathode. Electrons travel through the entire volume of the cathode and reach its surface. Oxygen is adsorbed in the cathode surface, and then reduced by the electrons. The oxygen ions created are further transported to the electrolyte via bulk path within the cathode.

A significant progress has been achieved in the last few years to develop new cathode materials based on the above-mentioned formula [3], but not many studies have been dedicated to investigate the influence of the microstructure on their properties.

The use of nanostructured materials has been shown to improve the electrochemical properties of electrolyte materials [11], and so their use on cathodes deserves to be investigated. Nowadays, nanostructured materials are not employed in conventional SOFCs, mainly because the grain size of the used materials increases at the high operation temperatures of SOFCs. However, their use in IT-SOFCs is currently under evaluation, since grain growth can be minimized for their working temperature range. Cathodes based on nanostructured mixed ionic/electronic conductors (MIECs) are particularly interesting because the number of active sites for the oxygen reduction is expected to increase dramatically due to the increase in the specific surface area. Fig. 1 shows a schematic representation of the processes occurring in MIEC cathodes. The idea is that the use of MIECs extends the reactive area much beyond the Triple Phase Boundaries (TPBs) and the use of nanostructures increases both the exposed area of the cathode and the number of TPBs. Thus, the net result is an overall increase on the availability of reactive points.

Recent results of our research group [12] and others [13,14] have shown that nanostructured cathodes of standard materials such as LSCO, exhibit similar or even better performance as cathodes than newly discovered materials [15,16].

At the present time, many techniques are available to develop different kinds of nanostructures, which in general are oriented to the miniaturization of devices. In the case of SOFCs electrodes, nanostructuring can be used to obtain highly porous films with large areas exposed to the surrounding environment. With this in mind, tubular nanostructures seem to be a good candidate to use in this kind of application. A simple method, that allows to obtain tubular nanostructures (nanotubes) consistent of agglomerated nanoparticles of several simple and complex oxides by pore wetting of polycarbonate porous membranes, has been proposed in the last few years [17,18].

We recently used this procedure to develop a novel architecture for SOFC cathodes [12,19]. The resulting area-specific resistance (ASR) of the cathode made with nanotubes is significantly lower than that corresponding to a microstructured one. As it has been explained above, this enhanced performance can be mainly attributed to the fact that this structure provides electrodes with high surface to volume ratio, increasing the number of reaction sites with the surrounding gas, when compared to an ordinary microstructured cathode. The synthesis method is extremely simple and allows to obtain nanotubes in a wide range of chemical compositions and sizes, so that a thorough study of the influence of both variables in the properties of the cathode can be performed.

In this work we study the electrochemical properties of cathodes made of LSCO nanotubes, focusing on understanding the influence of the geometry of the precursor nanotubes and the sintering conditions used to attach the cathode to the electrolyte. Our main objective is to obtain the optimum parameters to allow their application in practical devices.

2. Experimental procedure

A 1 M stoichiometric solution of $La(NO_3)_3{\cdot}6H_2O$, $Sr(NO_3)_2$ and $Co(NO_3)_2{\cdot}6H_2O$ was prepared by the dissolution of analytical reagents in pure water. To avoid the cobalt oxide precipitation the solution was maintained at acidic pH. Templates of porous polycarbonate films were used as filters in an adequate system for syringe filtration. By this process the total volume of the pores is filled with the solution. Commercial porous polycarbonate films were membrane filters from Millipore™. Membranes passing through holes of 100, 200, 400 and 800 nm diameter were used. In the following, samples with those nominal nanotube diameters will be denoted as LSC1, LSC2, LSC4 and LSC8, respectively.

The reaction to obtain the desired compound proceeds by the denitration process of the confined precursor in a microwave oven. By adjusting the time and the energy applied to the sample it is possible to accomplish this reaction without producing damage to the polycarbonate film. The perovskite compound LSCO is finally obtained and the template is sacrificed during a thermal treatment in a standard furnace at the final temperature of 800 °C. After 10 min at 800 °C the furnace goes freely to room temperature. The resulting material is a collection of sub-micrometric tubes whose diameter depends on the size of the pores of the template used. The LSCO compound can also be obtained by performing a thermal treatment at 750 °C, but the obtained nanotubes in this case are much fragile and thus less adequate considering the process needed to obtain the cathodes' precursor ink.

Electrolytes were prepared from commercial CeO_2–10 mol.% Sm_2O_3 powders (SDC, Nextech Materials™) by uniaxial pressing at 200 MPa and sintering at 1350 °C for 2 h, obtaining 0.5 mm thick samples with a relative density higher than 96%.

LSCO nanotubes were made into an ink for cathode deposition, using commercial ink vehicle (IV) from Nextech Materials™. We tested different LSCO/IV mass ratios in order to obtain the best film adherence. We made inks for all the samples, using a 1:2 LSCO:IV mass ratio in all cases, in order to optimize the viscosity of the ink and also to make equivalent samples to compare. We painted several samples with the ink made by each of our powders, to check reproducibility and also to compare the different procedures described above. Then we smeared this ink with a brush on the electrolyte to fabricate symmetrical LSCO/SDC/LSCO cells. Once painted, the samples were dried at 50 °C in air for about 20 min. Afterwards, two different processes were conducted to attach the cathode to the electrolyte:

- A fast firing process with dwell temperatures between 900 and 1200 °C and dwell times of 1–10 min, with heating and cooling rates of about 200 °C min^{-1}.
- A conventional sintering of 1 h at 1000 °C, with a heating and cooling rate of 10 °C min^{-1}.

The first method is expected to keep better the original hollow structure of the nanotubes, while the second was used to improve adherence of the film. In both cases, the electrode area was around 0.5 cm^2.

The area-specific resistance (ASR) of the cathodes was determined from Electrochemical Impedance Spectroscopy (EIS) measurements performed in air with a Solartron 1255 FRA and an EG&G Princeton Applied Research 273A potentiostat with silver paste as current collector. Measurements were performed at zero bias. Under these conditions our results were found to be highly reproducible.

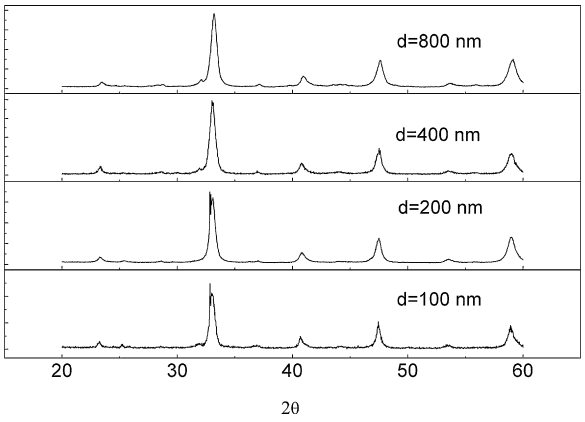

Fig. 2. X-ray powder diffraction data for samples with different tube diameters (d). All diagrams correspond to the typical perovskite-type structure of LSCO.

3. Results and discussion

In Fig. 2 our X-ray powder diffraction data for samples with different nominal tube diameters (d) are shown. In fact, the actual diameter of the nanotubes is slightly smaller due to contraction inside the pores of the template. We can see that they are all single phase, corresponding to a perovskite-type structure.

Crystallite sizes were determined from XRD patterns using the Scherrer formula. The values for all samples ranged from 15 to 20 nm approximately, showing no significant variation with the diameter of the tubes. No clear dependence was observed for the specific surface area of the powders, displaying values of 32, 18 and 56 $m^2\ g^{-1}$ for LSC2, LSC4 and LSC8 powders, respectively.

In Fig. 3 SEM micrographs of LSC2, LSC4 and LSC8 samples are shown in the same scale. All samples are comprised by hollow cylinders with dimensions corresponding to that of the pores of the template.

Firstly we tested the fast firing procedure to achieve the best possible adherence, changing the final temperature between 900 and 1200 °C, and the dwell time in the range from 60 to 600 s. The optimum condition was found with $T = 1100$ °C and $t = 60$ s (FF1100). These values have also been shown to result in a cathode with very good electrical properties [12].

The FF procedure has the advantage of being fast and to avoid significant grain growth of the nanostructure, but it could also result in a fragile and unstable cathode. For example, a significant fraction of the FF1100 cathode can be removed from the SDC surface by scraping a piece of paper. To make a cathode that overcomes these problems, we performed a standard sintering procedure on identically made samples. Our best results, in terms of adherence and with similar grain growth as that of FF1100, were obtained for a final temperature of 1000 °C and dwell time of 1 h (TT1000).

Table 1
Diameter (d), wall thickness (s) and crystallite size (cs) for the obtained cathodes.

Sample	d (nm)	s (nm)	cs (nm)
LSC2-FF1100	219 ± 47	–	65 ± 5
LSC4-FF1100	390 ± 51	–	75 ± 2
LSC8-FF1100	622 ± 77	162 ± 38	95 ± 5
LSC2-TT1000	145 ± 30	–	85 ± 2
LSC4-TT1000	358 ± 32	–	90 ± 10
LSC8-TT1000	605 ± 90	122 ± 29	130 ± 5

Fig. 4(a) and (b) displays SEM micrographs of LSC2, LSC4 and LSC8 (from left to right) sintered following the FF1100 and the TT1000 procedures, respectively. It can be observed that the resulting morphology for both procedures is very similar. A close inspection showed no trace of a hollow structure in LSC2 and on almost all of LSC4 cathode, for the TT1000 treatment. In the case of the FF1100 procedure, both LSC2 and LSC4 cathodes seem to be formed by dense rods of sub-micrometric dimension (nanorods). This clearly means that the increase of the particle size partially destroys the tubular shape of the powder.

The cross-section of the LSCO/SDC interface is shown in Fig. 5 for LSC4 and LSC8 corresponding to TT1000. The picture shows that the cathodes have a thickness of around 20 μm and a highly porous structure both at the meso- and nanoscales. The first is related to the separation between the nanotubes and the second, which is obviously absent for solid cylinders, to their intrinsic hollow structure.

The microstructural characteristics of each cathode, that arise from the analysis of SEM micrographs like the ones shown in Figs. 3 and 4, are summarized in Table 1. We also added the crystallite size obtained from XRD analysis of the electrodes.

The cathodes' performance was further investigated using EIS on symmetrical cells, measured in air. Fig. 6 shows the Nyquist plot for the cathode made with the LSC2 sample for temperatures in the range from 550 to 700 °C. In all cases we obtained one single arc, which is a signature of an impedance dominated by adsorption and diffusion [20]. ASR values were determined as the difference between the low frequency and the high frequency intercepts of the data with the real axis, indicated as LF and HF, respectively. The high frequency intercept is related to the total resistance of the SDC pellet.

Fig. 7 shows the ASR values as a function of temperature for cathodes made with the different samples, for both the FF1100 and the TT1000 procedures. A clear dependence with the tube diameter can be seen, unambiguously showing that the inks made with the smaller precursor nanotubes result in a best cathode.

In particular, at 700 °C all cathodes display good values for technological applications, reaching $0.19 \pm 0.01\ \Omega\ cm^2$ for the LSC1 sample attached following the TT1000 procedure. Even at 650 °C, the LSC2 samples have an ASR below $0.5\ \Omega\ cm^2$ for both procedures.

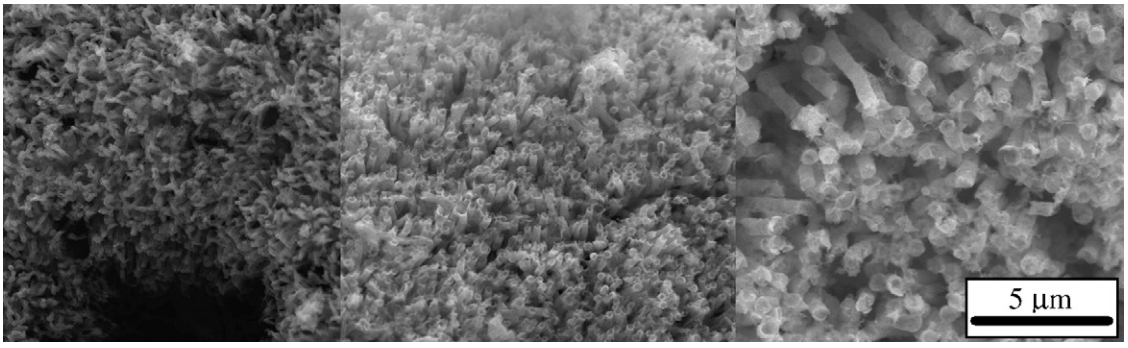

Fig. 3. SEM micrographs for (from left to right) LSC2, LSC4 and LSC8 samples, prior to the thermal treatment.

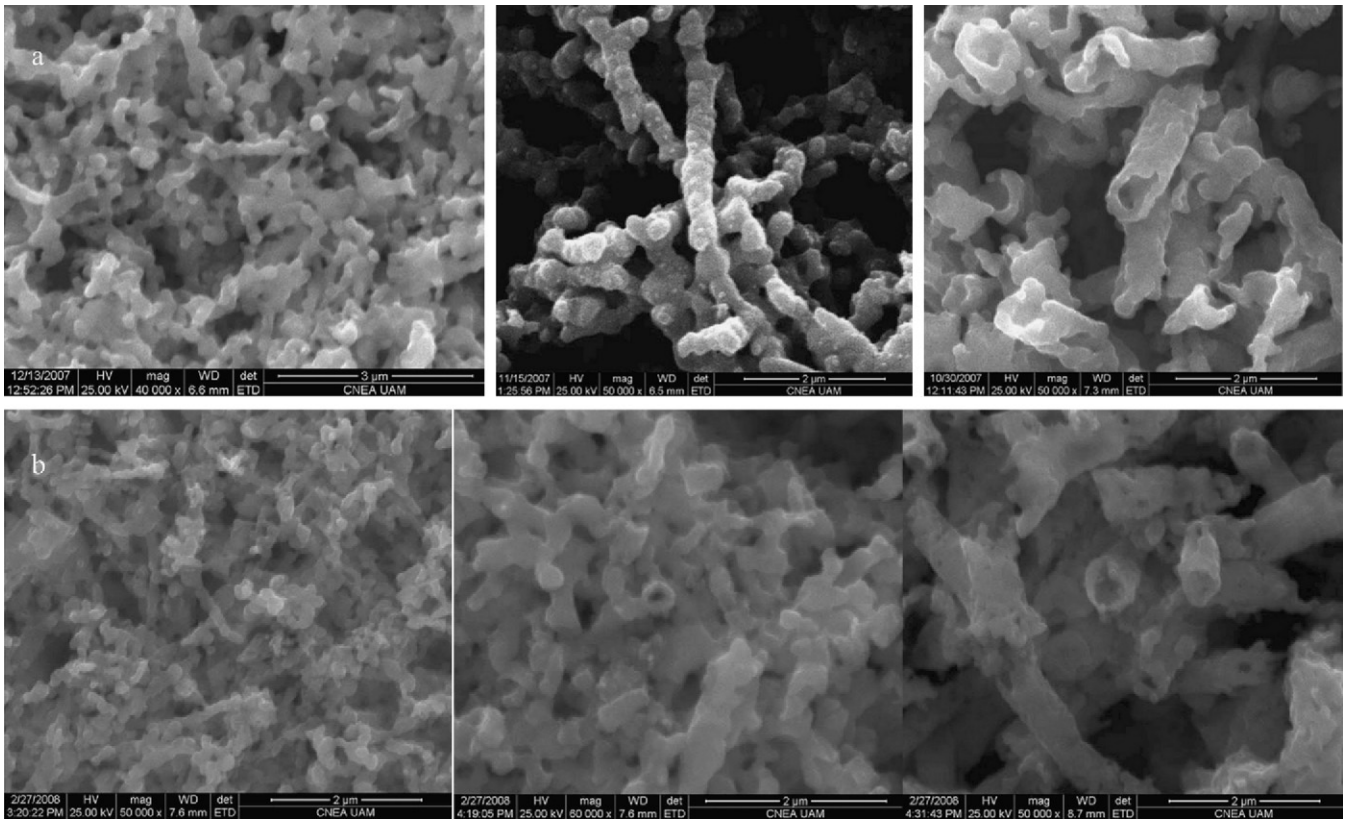

Fig. 4. SEM micrographs of (a) cathodes sintered following the fast firing procedure at 1100 °C and (b) cathodes sintered at 1000 °C for 1 h. In both cases cathodes obtained using LSC2, LSC4 and LSC8 are shown from left to right.

An enhancement can be seen from the LSC2 to the LSC1 cathode, but the resulting microstructure of the LSC1 cathode shows almost no evidence of the original nanotubes (see Fig. 8).

Both graphs of Fig. 7 are in the same scale, showing that the ASR of the cathodes has a slight dependence on the type of sintering procedure.

A simple model can address for the observed results. Lets consider for instance the structural characteristics of the LSC2 and the LSC8 cathodes for the TT1000 case (Table 1). We see that the whole diameter of the LSC2 tubes, after treatment, approximately fits into the walls of the LSC8 ones. A schematic picture is shown in Fig. 9 to clarify this idea. The thermal treatment causes a slight reduction of the diameter of the tubes and, in the case of LSC2, closes the cylindrical structure. As displayed in the figure, if we compare two cathodes with the same amount of LSCO mass but distributed as LSC2 and LSC8, the exposed surface area is significantly larger in the former case, which mean a large number of active sites for oxygen reduction. The LSC2 cathode thus results to have better conductivity. This picture is consistent with the fact that only one arc is observed in the impedance plots, a typical feature observed in cathodes dominated by processes such as oxygen surface exchange, solid-state diffusion, and gas phase diffusion [20]. The case of LSC4 is intermediate, as only a few of the tubes remained hollowed while almost all of them became cylinders as the SEM pictures showed.

We see in Fig. 10(a) that in the case of the LSC8, the fast-fired cathodes have higher ASR than the TT1000 ones and that this difference decreases for the tubes of smaller diameters. A possible reason for this behavior is the following: in the fast firing process, the structure of LSC8, in which the forming particles are much separated from each other than on the other samples due to curvature of the nanotube, is an obstacle to the sintering process. Thus it is likely that for the longer treatments like TT1000, significant sintering can be obtained for this sample when compared to the FF1100. For the other samples, the increased curvature of the surface tends to bring the particles close to each other downplaying the role of time in the sintering process.

A distinction has to be made in the case of tubes of small diameter (LSC1). The cathode obtained with LSC1 displays the lowest ASR reported in this work. The resulting structure of the LSC1 cathode shows no resemblance of the forming nanotubes, marking a qualitative difference against the other cathodes although it is evidently highly porous (see Fig. 8). We think that the main reason for this porosity has its origin in the use of the nanotubes. When they are smeared on the electrolyte they form a kind of "sponge" that preserves porosity even after sintering, because of the few contact points between nanotubes. Although it is pointless to search for such parameters as those presented in Table 1 on LSC1, the use of nanotubes seems to be preferred against other methods if a porous structure is likely to be beneficial, even in this case.

To gain further insight on the influence of geometry in the cathodes' performance, we have analyzed our EIS data in terms of the model developed by Adler, Lane and Steele (ALS) for LSCO porous cathodes [20,21]. The presence of a single arc in the Nyquist plot is consistent with an impedance co-limited by adsorption and gas phase diffusion dominated transport, which is expected for porous cathodes. In this case the impedance of the cathode is given by

$$Z_{chem} = R_{chem}\frac{1}{\sqrt{1+j\omega t_{chem}}}, \quad (1)$$

where R_{chem} and t_{chem}, are a characteristic resistance and time constant related to the thermodynamic, surface kinetics and transport properties of the mixed conductor.

Our data fits well with Eq. (1). In Fig. 10(b) and (c) we show the obtained fitting parameters as a function of the diameter of

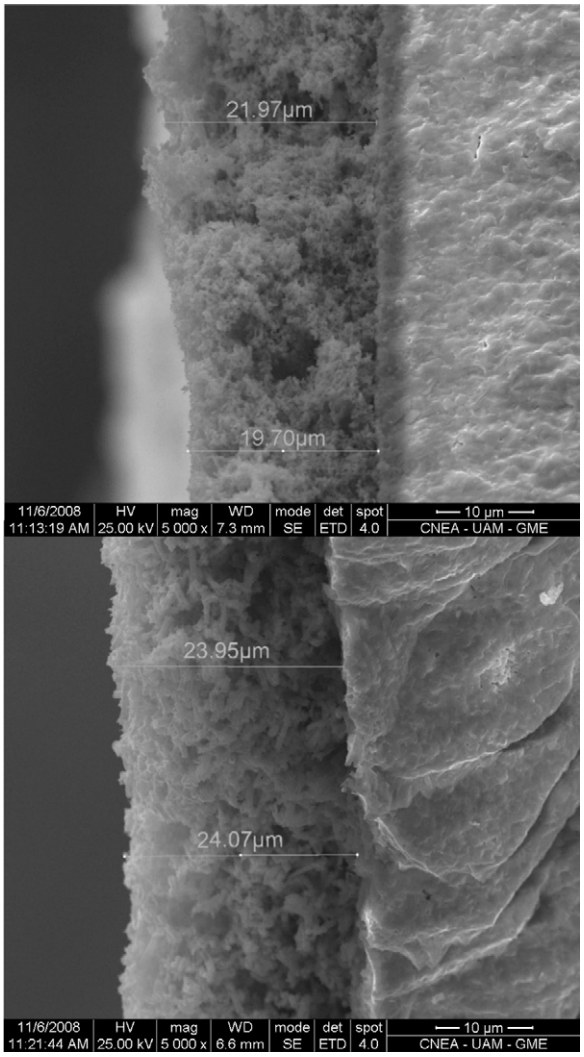

Fig. 5. Cross-sectional view of the cathodes made with (a) LSC4 and (b) LSC8 following the TT1000 procedure.

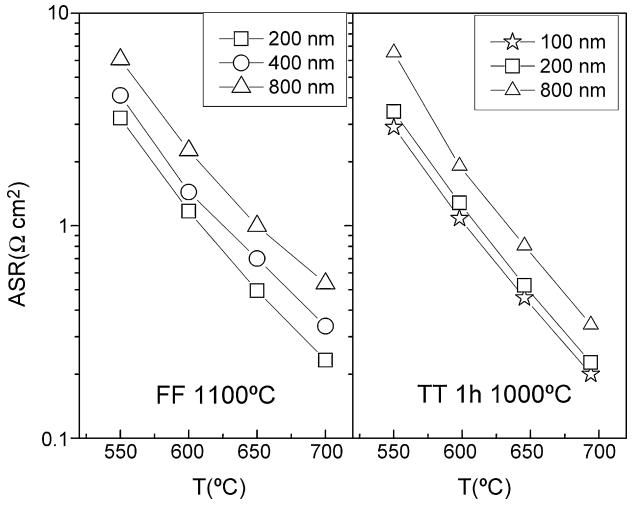

Fig. 7. Temperature dependence of the ASR values for several cathodes, following both attaching procedures.

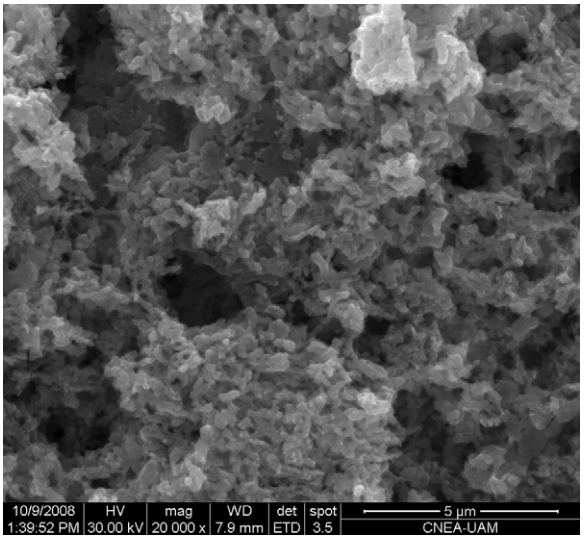

Fig. 8. SEM micrographs of the cathode made with LSC1, sintered at 1000 °C for 1 h. We see almost no evidence of the precursor nanotubes.

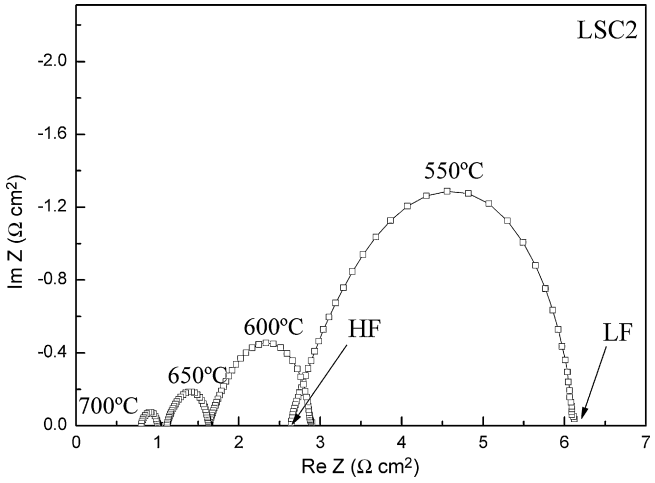

Fig. 6. Electrochemical Impedance Spectroscopy data for the LSC2 cathode sintered using the TT1000 procedure.

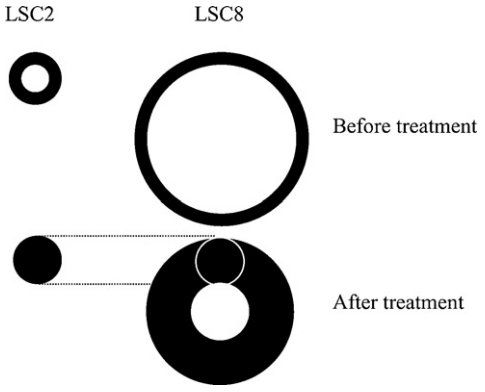

Fig. 9. Schematic representation of the tubes before and after the sintering process performed to attach the cathode to the electrolyte. The slight reduction of the outer diameter of the tubes is a consequence of sintering of the nanoparticles.

the precursor nanotubes. The increase of R_{chem} while increasing diameter resembles the behavior displayed in Fig. 10(a).

The dependence of t_{chem} has several interesting features. The oxygen vacancy diffusion coefficient is inversely proportional to t_{chem} [21], so the first important result that can be obtained from this figure is that in the TT1000 cathode, this mechanism is enhanced. We note that, for the TT1000 treatment, t_{chem} significantly decreases from 100 to 200 nm nanotubes and then slightly increases for 800 nm, showing an optimum diffusion for the LSC2 cathode and suggesting again the qualitative difference of the LSC1 one.

For the FF1100 procedure, the LSC2 cathode is also the one showing the minimum t_{chem}. An observed peculiarity is a maximum corresponding to the LSC4 cathode. We also show data of t_{chem} obtained for a cathode fast-fired at 1200 °C. We see an increase of the time constant for the FF1200 sample (as compared to the FF1100 one) that suggests a detriment of the diffusion process related with the increment of the grain size.

We have to point out that some authors tend to use a Warburg-type impedance [22] or even a simple RC equivalent circuit [23] to fit EIS data of cathodes of similar compositions. Both methods give the same two parameters described here (a characteristic resistance and a time constant) which have essentially the same interpretation presented here, but with distinct functional dependences. We tested these options and, in the case of the Warburg-type impedance, we obtained fittings of equivalent quality as those made with the ALS model, with similar values for the fitting parameters. We decided to use the ALS model because it is specifically developed for porous LSCO cathodes. However, the purpose of this work is not to test its validity against the other approaches, but just to extract the useful parameters and used them to describe the observed behavior. Although much work is needed to unambiguously determine which model is more appropriate to our case, the similar quality of the both fittings mentioned above suggests that diffusion is the most important limiting factor.

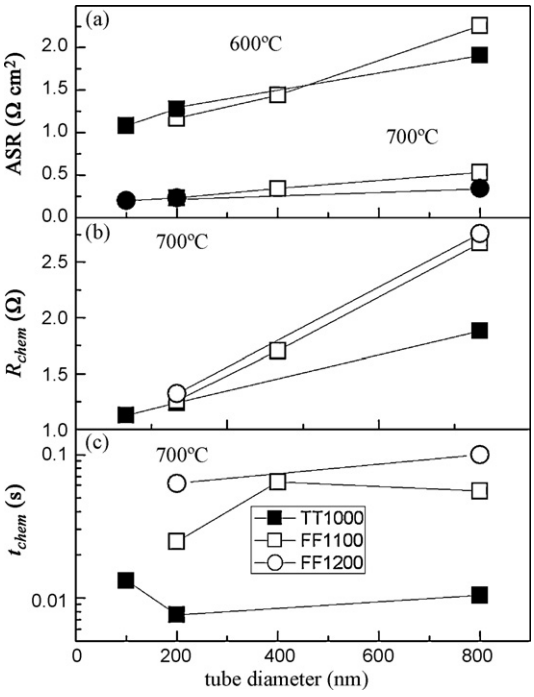

Fig. 10. (a) ASR values as a function of the nanotube diameter for 600 and 700 °C. Solid (open) symbols correspond to the TT1000 (FF1100) procedure (b) and (c) R_{chem} and t_{chem} obtained using the model proposed by Adler et al. [21], respectively (see text).

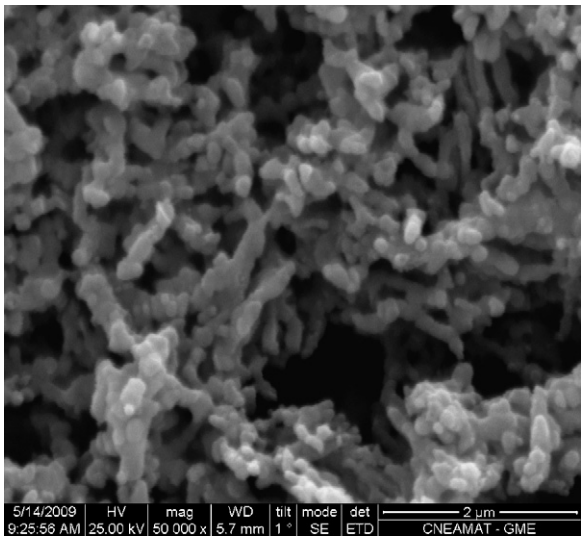

Fig. 11. SEM micrographs of the LSC2 TT1000 cathode after being measured at 600 °C for 500 h.

It is important to note that in none of the mentioned cases we observed the need for an additional high frequency contribution, but we cannot rule out the possibility of a small one. In any case, our data is clearly dominated by the low frequency contribution. This also suggests that the impedance is dominated by transport in a significant portion of the cathode volume [20].

Regarding the possibility of practical application of the cathodes we preliminary explored their long term stability. It has been recently shown that cathode degradation occurs in this compound [24]. The main result of the experiment was that percentual ASR change is almost temperature independent. It was proposed that the degradation mechanism is related with water adsorption on surface vacancies, mainly because its rate strongly depends on the humidity of the surrounding air.

We have measured the ASR for two samples kept at 600 and 700 °C, respectively for several cumulative times on the order of hundreds of hours. Our preliminary results showed that for $t \sim 100$ h, a change of around a 5% day^{-1} is obtained for the sample at 600 °C and a change of less than 4% day^{-1} for the one at 700 °C. This means that, if any, the dependence tends to decrease at higher temperatures. This result is reasonable if the degradation mechanism is related to the (temperature independent) creation of obstacles at the interfaces that have to be crossed. However, a deeper study of this dependence is necessary in order to clarify this behavior.

We also present a SEM image of the LSC2 TT1000 cathode, after been measured for 500 h at 600 °C (Fig. 11). It can be noted that, even though the resistivity of this sample has been significantly increased, no clear changes can be detected after the long thermal treatment, when compared with the previous image of the cathode (Fig. 4(b)).

4. Conclusions

As a summary of the present work, we have presented a study of solid oxide fuel cell cathodes, made with nanotubes of LSCO cobaltites, mainly focusing in the microstructure effect of the used powder.

The polarization resistance of the obtained cathodes is promising to use them on IT-SOFC. We found that the ASR has no significant dependence on whether a fast or a slow and long thermal treatment was performed to attach the cathode. However, an improvement in the diffusion mechanism was obtained in the case of a conven-

tional thermal treatment, probably related to a better adherence between the nanotubes themselves and with the electrolyte.

Our results showed that nanotubes with diameter around 200 nm or less are the best candidates to use, as they result in cathodes with the lower polarization resistance. However, we have to point that if the diameter of the nanotubes is very small (as for example 100 nm), the tubular structure can disappear after the attaching procedure, thus deteriorating adsorption and gas phase diffusion.

In the case of the cathode made with LSC2, the increase of grain size induced by the thermal treatments, causes that the original tubes became dense nanorods. We developed a qualitative model that successfully explains why this cathode exhibits a better performance than those formed by hollow tubes of larger diameter, for a given thermal treatment. The reason for this enhancement is that in the former case, a greater fraction of material is surrounded by gas, thus improving oxygen exchange.

We also showed that the fast firing process seems to be inadequate if large tubes, as LSC8 are used, but the difference tends to disappear while decreasing the diameter of the tubes.

Moreover, our results show that the slow sintering (TT1000) is preferable in order to favor the sintering process of the cathode and also to improve adsorption and gas phase diffusion.

We also obtained that oxygen vacancy diffusion seems to be enhanced for nanotubes of smaller particle sizes, this fact can be related with the improvement of ionic transport recently observed in nanostructured SOFC electrolytes [11]. Further work is needed to elucidate this point.

The great performance of the obtained cathodes with LSCO nanotubes, strongly suggests the study of this novel structure with newly discovered compounds for SOFC cathodes, as well as with materials for other applications in which the number of reaction sites with the surrounding environment is crucial. In this sense, we are currently working on the use of $Ba_{0.5}Sr_{0.5}Co_{0.8}Fe_{0.2}O_3$ nanotubes and other cobaltites as IT-SOFC cathode, and on their use in anode materials and catalysts [25].

Acknowledgments

The authors thank L. Granja, A. Petragalli, P. Bozzano and R. Kempf for their valuable help. Present address of M.G. Bellino is at Gerencia de Química, Centro Atómico Constituyentes, CNEA, San Martín, Argentina. This work has been supported by ANPCyT (PICT Nos. 14268 and 13517), CONICET (PIP No. 6559) and the Universidad Nacional de San Martín (SA06/078). J. Sacanell and D.G. Lamas are also members of CIC-CONICET.

References

[1] B.C.H. Steele, A. Heinzel, Nature 414 (2001) 345.
[2] S. Kartha, P. Grimes, Phys. Today 47 (1994) 54–61.
[3] S.C. Singhal, K. Kendal, High-Temperature Solid Oxide Fuel Cells: Fundamentals, Design and Applications, Elsevier, 2003.
[4] N.P. Brandon, S. Skinner, B.C.H. Steele, Annu. Rev. Mater. Res. 33 (2003) 183.
[5] Y. Takeda, R. Kanno, M. Noda, O. Yamamoto, Bull. Inst. Chem. Res. 64 (1986) 157.
[6] H. Uchida, S. Arisaka, M. Watanabe, Solid State Ionics 135 (2000) 347–351.
[7] A. Petric, P. Huang, F. Tietz, Solid State Ionics 135 (2000) 719–725.
[8] S.J. Skinner, Int. J. Inorg. Mater. 3 (2001) 113.
[9] Y. Takeda, R. Kanno, M. Noda, Y. Tomida, O. Yamamoto, J. Electrochem. Soc. 134 (1987) 2656.
[10] A. Ringuedé, J. Fouletier, Solid State Ionics 139 (2001) 167–177.
[11] M.G. Bellino, D.G. Lamas, N.E. Walsöe de Reca, Adv. Funct. Mater. 16 (2006) 107; M.G. Bellino, D.G. Lamas, N.E. Walsöe de Reca, Adv. Mater. 18 (2006) 3005.
[12] M.G. Bellino, J.G. Sacanell, D.G. Lamas, A.G. Leyva, N.E. Walsöe de Reca, J. Am. Chem. Soc. 129 (2007) 3066–3067.
[13] J. Yoon, R. Araujo, N. Grunbaum, L. Baqué, A. Serquis, A. Caneiro, X. Zhang, H. Wang, Appl. Surf. Sci. 254 (2007) 266–269.
[14] L. Baqué, A. Caneiro, M.S. Moreno, A. Serquis, Electrochem. Commun. 10 (2008) 1905–1908.
[15] Z. Shao, S. Haille, Nature 431 (2004) 170–173.
[16] J.H. Kim, S.-W. Baek, C. Lee, K. Park, J. Bae, Solid State Ionics 179 (2008) 1490–1496.
[17] P.P. Levy, A.G. Leyva, H.E. Troiani, R.D. Saĭnchez, Appl. Phys. Lett. 83 (2003) 5247–5249.
[18] A.G. Leyva, P. Stoliar, M. Rosenbusch, V. Lorenzo, P. Levy, C. Albonetti, M. Cavallini, F. Biscarini, H.E. Troiani, J. Curiale, R.D. Sanchez, J. Solid State Chem. 177 (2004) 3949–3953.
[19] J. Sacanell, M.G. Bellino, D.G. Lamas, A.G. Leyva, Physica B 398 (2007) 341–343.
[20] S.B. Adler, Chem. Rev. (2004) 4791–4843.
[21] S.B. Adler, J.A. Lane, B.C.H. Steele, J. Electrochem. Soc. (1996) 3554–3564.
[22] N. Grunbaum, L. Dessemond, J. Fouletier, F. Prado, A. Caneiro, Solid State Ionics 177 (2006) 907–913.
[23] T. Kawada, J. Suzuki, M. Sase, A. Kaimai, K. Yashiro, Y. Nigara, J. Mizusaki, K. Kawamura, H. Yugami, J. Electrochem. Soc. 149 (2002) E252–E259.
[24] P. Hjalmarsson, M. Sogaard, M. Mogensen, Solid State Ionics 179 (2008) 1422–1426.
[25] R.O. Fuentes, L.M. Acuña, M.G. Zimicz, D.G. Lamas, J. Sacanell, A.G. Leyva, R.T. Baker, Chem. Mater. 20 (2008) 7356–7363.